

Transformed composite sequences for improved qubit addressing

J. True Merrill,^{1,2,*} S. Charles Doret,^{1,†} Grahame Vittorini,^{3,‡} J. P. Addison,³ and Kenneth R. Brown^{2,3,4}

¹Georgia Tech Research Institute, Atlanta, Georgia 30332, USA

²School of Chemistry and Biochemistry, Georgia Institute of Technology, Atlanta, Georgia 30332, USA

³School of Physics, Georgia Institute of Technology, Atlanta, Georgia 30332, USA

⁴School of Computational Science and Engineering, Georgia Institute of Technology, Atlanta, Georgia 30332, USA

(Received 3 February 2014; published 2 October 2014)

Selective laser addressing of a single atom or atomic ion qubit can be improved using narrow-band composite pulse sequences. We describe a Lie-algebraic technique to generalize known narrow-band sequences and introduce sequences related by dilation and rotation of sequence generators. Our method improves known narrow-band sequences by decreasing both the pulse time and the residual error. Finally, we experimentally demonstrate these composite sequences using $^{40}\text{Ca}^+$ ions trapped in a surface-electrode ion trap.

DOI: [10.1103/PhysRevA.90.040301](https://doi.org/10.1103/PhysRevA.90.040301)

PACS number(s): 03.67.Pp, 03.67.Lx, 32.80.Qk, 37.10.Ty

In ion traps [1,2] and neutral atom optical lattices [3,4], single-qubit addressing typically requires focused lasers where the beam waist is smaller than the interatom separation. Closely spaced atoms are desirable to improve two-qubit coupling rates, often demanding interatom spacings approaching the diffraction limit. In practice, single-qubit addressing requires precise focal alignment and ultrastable beam steering to prevent unwanted excitations on neighboring atoms, a significant challenge as the number of qubits increases [5]. Furthermore, achieving the required tight focus is often made difficult by geometric constraints and restricted optical access [6,7]. These factors combine to make single-qubit addressing a challenge in many experimental systems.

Single-qubit addressing can be improved by the application of auxiliary fields to generate spatially dependent Zeeman and Stark shifts [8–13]. Quantum control has been used in conjunction with these frequency shifts to achieve addressing with inhomogeneous control fields [14]. A recent proposal also examined spatial refocusing through precise laser positioning coupled with controlled phase shifts [15]. These methods require time-consuming calibrations to remove systematic errors while adding to experimental complexity and are often designed for a specific experimental implementation.

In this Rapid Communication we demonstrate an alternative control scheme that replaces simple single-qubit gates with a narrow-band composite sequence of laser pulses designed for local addressing [16,17]. These sequences allow the exclusive manipulation of a single qubit even when neighboring qubits are subjected to significant laser intensity, without required auxiliary fields. Such compensating sequences reduce systematic control errors at the cost of increasing gate times [17]. Our main result is a technique to generate fully compensating narrow-band sequences using Lie-algebraic transformations of other known sequences. We use numerical minimization to identify sequences with superior error correction properties and low operation times compared to the original sequence

family. Further, we demonstrate the effectiveness of these sequences in an experiment with $^{40}\text{Ca}^+$ ion qubits in a surface-electrode trap.

We consider a register of N identical spatially separated qubits. A resonant laser in the rotating-wave limit illuminates an addressed qubit i , but also illuminates neighboring qubits j at a lower intensity, resulting in an addressing error. Control over the qubits is implemented by applying a time-dependent Hamiltonian

$$H(t) = \frac{\hbar\Omega_i}{2} \left\{ \sigma_i(\varphi(t)) + \sum_{j \neq i} \epsilon_j \sigma_j(\varphi(t)) \right\}, \quad (1)$$

where $\varphi(t)$ is the laser phase, Ω_i is the Rabi frequency for the addressed qubit i , and $\sigma(\varphi(t)) = X \cos \varphi(t) + Y \sin \varphi(t)$, where X and Y are Pauli operators. For simplicity we fix $|\Omega_i|^2$ to a maximal value corresponding to the intensity peak of the laser field. The terms $\epsilon_j \sigma_j(\varphi(t))$ induce undesired correlated rotations on neighboring qubits. Here the ratio $\epsilon_j = \Omega_j/\Omega_i < 1$, where Ω_j is the Rabi frequency at the neighboring qubit j . The frequency Ω_j parametrizes the magnitude of the addressing error and is assumed to be fixed over the entire duration of the control. The time dependence of $H(t)$ is entirely due to the temporal modulation of the phase $\varphi(t)$.

Compensating pulse sequences choose $\varphi(t)$ to yield a net evolution robust against a particular class of systematic errors. A common simplification for $\varphi(t)$ is to divide the time coordinate into L time intervals $(\Delta t_1, \Delta t_2, \dots, \Delta t_L)$ for which the phase is a constant angle $(\varphi_1, \varphi_2, \dots, \varphi_L)$. Each pulse applies a spin rotation controlled by the generator of rotations $r_\ell = -i\theta_\ell \sigma(\varphi_\ell)/2$, where $\theta_\ell = \Omega_i \Delta t_\ell$ is the pulse area or rotation angle applied to the addressed qubit. The total propagator for the entire sequence is $U(\mathbf{r}) = U_i(\mathbf{r})[\otimes_{j \neq i} U_j(\mathbf{r})]$ where

$$U_i(\mathbf{r}) = \prod_{\ell=1}^L \exp(r_\ell), \quad U_j(\mathbf{r}) = \prod_{\ell=1}^L \exp(\epsilon_j r_\ell) \quad (2)$$

are the gates applied to the addressed qubit i and the neighbor qubit j , respectively, and $\mathbf{r} = (r_1, r_2, \dots, r_L)$ is the ordered set of rotation generators. With a careful choice of rotation generators, it is possible to produce propagators that apply a nontrivial gate $U_i(\mathbf{r}) = U_T$ to the addressed qubit while

*true.merrill@gtri.gatech.edu

[†]Present address: Department of Physics, Williams College, Williamstown, MA 01267, USA.

[‡]Present address: Joint Quantum Institute and Department of Physics, University of Maryland, College Park, MD 20742, USA.

simultaneously approximating the identity $U_j(\mathbf{r}) = I + O(\epsilon_j^{n+1})$ on all neighboring qubits. Sequences with this property are called n th-order fully compensating narrow-band sequences [16–19]. So long as $\Omega_j \ll \Omega_i$ these sequences reduce errors on all unintentionally illuminated qubits.

We remark that an n th-order narrow-band sequence must satisfy a set of n Lie-algebraic constraints on the rotation generators. Applying the Baker-Campbell-Hausdorff lemma we find that $U_j(\mathbf{r}) = \exp\{\sum_{m=1}^{\infty} \epsilon_j^m F_m(\mathbf{r})\}$, where $F_m(\mathbf{r})$ is given by the generators and their commutators and is related to the m th-order average Hamiltonian. Explicitly the first two terms are

$$F_1(\mathbf{r}) = \sum_{\ell=1}^L r_{\ell}, \quad F_2(\mathbf{r}) = \frac{1}{2} \sum_{\ell=1}^L \sum_{k=1}^{\ell} [r_{\ell}, r_k]. \quad (3)$$

To satisfy $U_j = I + O(\epsilon_j^{n+1})$ for all values of ϵ_j , each $F_m(\mathbf{r})$ with $m \leq n$ must independently equal zero. Frequently it is possible to assign a geometric interpretation to each constraint. For example, $F_1(\mathbf{r}) = 0$ requires the generators \mathbf{r} to form a closed figure on the Lie algebra, and $F_2(\mathbf{r}) = 0$ requires that the figure encloses signed areas of equal magnitude but opposite sign.

We introduce a method to generalize existing narrow-band sequences by identifying Lie-algebraic transformations on the generators which leave the constraint equations satisfied. These transformations yield derivative sequences which achieve the same order of error suppression, but may offer substantial improvements in the total composite gate time as well as the gate accuracy. Our method can be described as follows. Let $\mathcal{T}_{\lambda} : \text{su}(2) \mapsto \text{su}(2)$ be a map between Lie algebra elements with the condition that if $F_m(\mathbf{r}) = 0$, then $F_m(\mathcal{T}_{\lambda} \circ \mathbf{r}) = 0$ for all $m \leq n$. This ensures that if \mathbf{r} generates an n th-order compensating sequence, then $\mathbf{r}(\lambda) = \mathcal{T}_{\lambda} \circ \mathbf{r}$ also generates a sequence of the same order; however, in general, $U_i(\mathbf{r}(\lambda)) \neq U_i(\mathbf{r})$. To find sequences that implement a particular target gate U_T , we perform an optimization over the mapped sequences to minimize a cost functional while constraining $U_i(\mathbf{r}(\lambda)) = U_T$. Two cost functionals we consider are the total pulse area $\theta_{\text{total}} = \sum_{\ell} |\theta_{\ell}|$, related to the total time required to perform a composite gate, and the infidelity of the effective identity gate on the neighboring qubits $\mathcal{I}(I) = 1 - \mathcal{F}(I, U_j(\mathbf{r}(\lambda)))$, where $\mathcal{F}(V, U) = |\text{tr}[V^{\dagger}U]|/2$ is the fidelity between gates V and U .

Maps that satisfy the constraint condition are common affine transformations. For arbitrary sequences, compositions of rotations and dilations fulfill the requirement: $F_m(R\mathbf{r}R^{\dagger}) = RF_m(\mathbf{r})R^{\dagger}$ and $F_m(\lambda\mathbf{r}) = \lambda^m F_m(\mathbf{r})$. Independent dilation of each axis $\mathcal{T}_{\lambda_x} \circ X = \lambda_x X$ and $\mathcal{T}_{\lambda_y} \circ Y = \lambda_y Y$ will also satisfy this criteria for $n \leq 2$, and in our case, where the controls are restricted to the X - Y plane, for $n \leq 3$. Starting with an initial seed sequence \mathbf{r} we generate a family of related sequences $\mathbf{r}(\lambda_x, \lambda_y, R)$ by the composition of dilations and rotations (Fig. 1).

As an example, consider the first-order pass-band SK1 pulse sequences, produced by the generators $\mathbf{r}_{\text{SK1}}(\theta) = (-i\theta\sigma(0)/2, -i\pi\sigma(\varphi_{\text{SK1}}), -i\pi\sigma(-\varphi_{\text{SK1}}))$ where $\cos \varphi_{\text{SK1}} = \theta/(4\pi)$ [18]. On the addressed qubit SK1 applies $U_i(\mathbf{r}_{\text{SK1}}(\theta)) = \exp(-i\theta X/2)$ and it approximates the identity on neighboring qubits, $U_j(\mathbf{r}_{\text{SK1}}(\theta)) = I + O(\epsilon_j^2)$. To illustrate

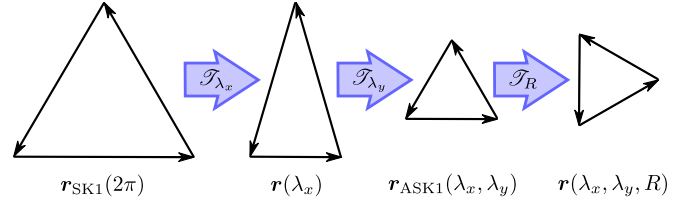


FIG. 1. (Color online) Construction of $\mathbf{r}_{\text{ASK1}}(\lambda_x, \lambda_y)$ by compositions of dilation and rotation maps applied to $\mathbf{r}_{\text{SK1}}(2\pi)$.

our transformation method, we start with the specific case $\mathbf{r}_{\text{SK1}}(2\pi)$ and identify a map which recovers the entire SK1 family. Let \mathcal{T}_{θ} be the one parameter map that contracts the X components by $\lambda_x = \theta/(2\pi)$ and expands the Y components by $\lambda_y = \sqrt{(4 - \lambda_x^2)}/3$. This map satisfies $F_1(\mathcal{T}_{\theta} \circ \mathbf{r}_{\text{SK1}}(2\pi)) = 0$ and $\mathbf{r}_{\text{SK1}}(\theta) = \mathcal{T}_{\theta} \circ \mathbf{r}_{\text{SK1}}(2\pi)$.

SK1 can implement an arbitrary single-qubit gate using extra rotations, $U_T = RU_i(\mathbf{r}_{\text{SK1}}(\theta))R^{\dagger}$. Alternatively, one simply changes the sequence generators using the similarity transformation $\mathbf{r}_{\text{SK1}}(\theta, R) = R\mathbf{r}_{\text{SK1}}(\theta)R^{\dagger}$. For a target in-plane rotation $U_T = \exp(-i\theta\sigma(\varphi_T)/2)$ this can be achieved by advancing all the φ_i in SK1 by φ_T .

The composition of independent X and Y dilation maps applied to $\mathbf{r}_{\text{SK1}}(2\pi)$ generates a larger family of narrow-band sequences that we call ASK1, $\mathbf{r}_{\text{ASK1}}(\lambda_x, \lambda_y) = \mathcal{T}_{\lambda_y} \circ \mathcal{T}_{\lambda_x} \circ \mathbf{r}_{\text{SK1}}(2\pi)$. Figure 1 illustrates the construction of ASK1 sequences. Note that ASK1 usually applies a net rotation $U_i(\mathbf{r}_{\text{ASK1}}(\lambda_x, \lambda_y))$ about an axis outside of the X - Y plane; such a sequence cannot replace an in-plane rotation implemented by a single resonant pulse with a constant phase. To achieve a target in-plane gate U_T , we introduce the similarity transformation $\mathbf{r}_{\text{ASK1}}(\lambda_x, \lambda_y, R) = R\mathbf{r}_{\text{ASK1}}(\lambda_x, \lambda_y)R^{\dagger}$, where $U_T = U_i(\mathbf{r}_{\text{ASK1}}(\lambda_x, \lambda_y, R))$. We decompose $R = \exp(r')T$, where $\exp(r')$ applies the minimum-angle rotation to match the polar angle of the rotation axis; T is a rotation about Z which can be implemented by a uniform phase advance on the inner ASK1 pulses. This transformed sequence construction, which we call TASK1, sets the net rotation angle with the innermost pulses. In terms of rotation generators the sequence is $\mathbf{r}_{\text{TASK1}}(\lambda_x, \lambda_y, R) = (r', T\mathbf{r}_{\text{ASK1}}(\lambda_x, \lambda_y)T^{\dagger}, -r')$. A global phase advance controls the azimuthal angle of the net rotation axis.

Despite the inclusion of two additional pulses, the TASK1 sequences outperform SK1. Figure 2(a) shows the TASK1 family in terms of (λ_x, λ_y) and plots contours of the net rotation angle and total pulse area. Using constrained optimization we identify a subfamily of sequences that minimize the total pulse area, TASK1 (T_{min}), and the infidelity, TASK1 (E_{min}) for a fixed net rotation angle. The error-minimal sequences correspond to $\lambda_x = \lambda_y$ and result in ASK1 sequences homologous to equilateral triangles in $\text{su}(2)$. Figure 2(b) compares the infidelity and total pulse area for each sequence subfamily. TASK1 (T_{min}) and TASK1 (E_{min}) outperform SK1 in both the required time and the minimization of the residual rotation on the neighboring qubit and both sequences yield similar performance for most net rotation angles. In particular, for a target rotation $U_T = \exp(-i\pi X/2)$, the error-minimal and time-minimal sequences are identical, $\lambda_x = \lambda_y = 1/2$, and TASK1 performs the gate using 3/5 of the total pulse area and

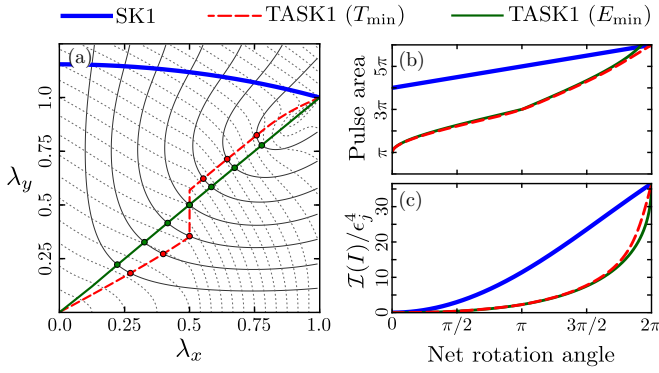


FIG. 2. (Color online) (a) Narrow-band TASK1 family in terms of the scale parameters (λ_x, λ_y) . TASK1 sequences implement $U_T = \exp(-i\theta X/2)$ on addressed qubits; θ is the net rotation angle. Contours of θ (solid) and θ_{Total} (dashed) are plotted in intervals of $\pi/4$. SK1 sequences (blue, thick solid) are a subfamily of TASK1. (b) TASK1 (T_{min}) (red, dashed) is the subfamily which minimizes θ_{Total} . (c) TASK1 (E_{min}) (green, solid) minimizes $\mathcal{I}(I)$.

with 1/5 of the residual infidelity compared to SK1. Explicit descriptions of the pulses can be found in the Supplemental Material [20].

We demonstrate these sequences by addressing individual $^{40}\text{Ca}^+$ ions confined in a microfabricated surface-electrode trap [7]; details of our surface trap setup can be found in [21]. We use a 397 nm laser to Doppler cool and optically pump ions into the $|1\rangle = ^2S_{1/2} (m_j = -1/2)$ state. A narrow linewidth ($\gamma \sim 150$ Hz) 729 nm laser tuned to the $|1\rangle \rightarrow |0\rangle = ^2D_{5/2} (m_j = -5/2)$ qubit transition is used to sideband cool the ion to ≤ 0.1 phonons in all motional modes and to perform subsequent qubit rotations. The 729 nm beam propagates parallel to the trap surface, intersecting the trap symmetry plane at a 45° angle with a $w_0 = 44.2 \pm 0.8 \mu\text{m}$ $1/e^2$ diameter waist. Laser switching and phase control is achieved using an acousto-optic modulator driven by a 16-bit direct-digital synthesizer with 20 ns timing resolution. After applying a sequence of laser pulses, we measure the $|1\rangle$ state population using laser-induced fluorescence.

We verify our theoretical predictions for TASK1 sequences by measuring the qubit state transfer for differing pulse areas, controlled by adjusting the timings of each laser pulse to scale the energy-time product by a constant multiple ϵ_j . The resulting propagation is equivalent to the evolution that would be experienced during an addressing error by neighboring ions over differing laser intensities. Figures 3(a) and 3(b) compare the measured response for pulse sequences applying $U_T = -iX$ and $U_T = \exp(-i\pi X/4)$, respectively, to a target ion. We observe that unwanted population inversion is suppressed when $\epsilon_j < 1$, as desired and when $\epsilon_j \simeq 1$ the observed state transfer is consistent with the expected gate. We find excellent agreement between the calculated and measured responses as a function of pulse area.

We observe addressing error compensation by measuring the state transfer as a function of ion position relative to the center of the addressing beam [Fig. 3(c)]. The ion position along the trap axis is controlled to better than $\pm 0.5 \mu\text{m}$ by biasing a subset of 46 segmented dc trap electrodes [7]. We find that TASK1 sequences exhibit predicted narrow-band behavior:

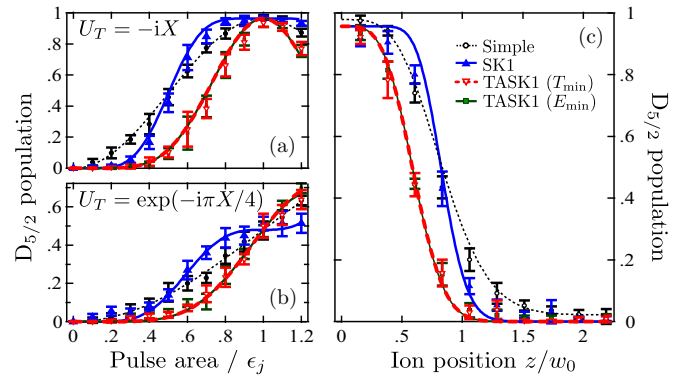


FIG. 3. (Color online) Population inversion as a function of normalized pulse area ϵ_j for (a) $U_T = -iX$ and in (b) $U_T = \exp(-i\pi X/4)$, and as a function of ion position for (c) $U_T = -iX$. Shown are simple rotations (black, dotted), SK1 (blue, thick solid), TASK1 (T_{min}) (red, dashed), and TASK1 (E_{min}) (green, solid). Curves are theoretical predictions with a single, common adjustable parameter accounting for experimental qubit detection fidelity.

Unwanted rotations on ions far from the beam are suppressed, while at the beam center the desired rotation is executed. SK1 sequences are pass-band [18] and simultaneously reduce the sensitivities of the target gate to position uncertainty and the unwanted rotation on the neighboring qubit [17].

To quantify the gain of these techniques in terms of ion spacing, we calculate the theoretical fidelity of the applied gate with respect to both the I gate [Fig. 4(a)] and the $-iX$ gate [Fig. 4(b)] as a function of position from the center of a Gaussian beam with waist w_0 . For a target infidelity on the neighboring ion $\mathcal{I}(I) \leq 10^{-4}$, we find the ion separation must be greater than $2.172w_0$ for the simple pulse, $1.704w_0$ for SK1, and $1.584w_0$ for TASK1 (T_{min}).

We also compare pulse sequence techniques to addressing methods that uses auxiliary field gradients [8–10]. To facilitate comparison between the methods, we require a gradient as large as $\Delta/z \geq 1.137 \Omega/w_0$, where Δ is the applied shift in the qubit resonance frequency. At this strength, the gradient method produces an identity gate with infidelity $\mathcal{I}(I) \leq 10^{-4}$ on the neighboring qubits while simultaneously performing $-iX$ on the addressed qubit with the same ion separation and gate time as TASK1 (T_{min}). For our setup, where the beam waist is intentionally large to reduce the fractional positioning error

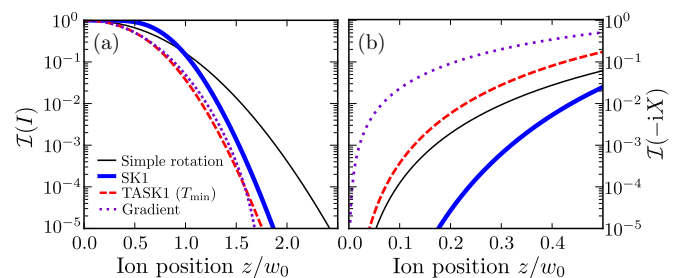


FIG. 4. (Color online) Gate infidelity as a function of ion position compared to (a) the identity operation and (b) $U_T = -iX$ gates composed of a simple rotation, TASK1 family pulses, or a simple rotation with a qubit frequency gradient (see text).

in z/w_0 , this corresponds to a modest magnetic field gradient of 90 mT/m. However with diffraction limited optical beams and $\Omega = 1$ MHz Rabi frequency the required gradient is as large as 111 T/m. As a point of comparison, strong gradients of 20 T/m have been achieved with permanent magnets [22] and on-chip currents have yielded static gradients of 0.06 T/m [10] and microwave gradients of 35 T/m [13]. Gates performed using the gradient technique are also more sensitive to ion positioning errors. To apply a $-iX$ gate to the target ion with infidelity $\mathcal{I}(-iX) \leq 10^{-4}$ requires positioning the ion to $z/w_0 \leq 0.0071$ for the gradient technique but for TASK1 (T_{\min}) the ion positioning tolerance is $z/w_0 \leq 0.072$.

Throughout our analysis we have assumed the laser beam position is fixed. Fluctuations in laser beam position lead to errors on the addressed qubit, where the amplitude depends quadratically on the beam displacement ζ , and reduce the error cancellation properties of the composite pulse on the neighboring qubits, where the amplitude has a linear dependence on ζ . For slow fluctuations relative to the pulse time, the cancellation properties of composite pulses are retained [23]. For an adversarial noise that switches the laser position in time with the pulses, the infidelity of the addressed qubit scales as $(\zeta/w_0)^4$ and the infidelity of the neighboring qubit at position z scales as $(\epsilon_j z \zeta / w_0^2)^2$. With adversarial noise to achieve an infidelity dominated by the residual term of the composite pulse, $\propto \epsilon_j^4$, then $\zeta/w_0 < \epsilon_j w_0 / z$. The fidelity of the neighboring qubit places a fractionally tighter bound on the pointing stability than the fidelity of the addressed qubit. We emphasize that this is a worst-case scenario and that for position instabilities uncorrelated with the pulse sequence this error will be significantly averaged away.

In conclusion, we introduced a Lie-algebraic transform method to produce narrow-band sequences from other known sequences. Using the technique, we developed the TASK1 family from transformations of SK1 and demonstrated their suitability for single-qubit addressing in an experiment with trapped ions. The TASK1 family results in improved total pulse area and error suppression. Our transformation method is well suited for narrow-band sequences, where there is no desired unitary operation on the neighboring qubits. Application of the mapping technique to other narrow-band sequences, e.g., NB1 and the $N2j$ family [18,24], is straightforward. Applying the technique to sequences where the errors occur on the addressed qubit, e.g., detuning and amplitude errors, should also be possible; however, there is additional complexity due to the control rotating the errors to a toggled frame [17]. In these cases Lie-algebraic maps cannot consist only of dilations but must also account for the frame transformation. Further, it is possible to concatenate these pulses with additional sequences that correct detuning errors. These concatenated sequences should also assist with addressability concerns in systems with variable splitting frequencies, such as superconducting qubits [25].

The authors thank J. M. Amini, A. M. Meier, and Kenton R. Brown for helpful discussions and critical review of the manuscript. G.V. and S.C.D. thank GTRI Shackelford Fellowships for graduate and postdoctoral support, respectively. This work was supported by the Office of the Director of National Intelligence, Intelligence Advanced Research Projects Activity through Army Research Office Contract No. W911NF-10-1-0231 and Department of Interior Contract No. D11PC20167.

-
- [1] J. I. Cirac and P. Zoller, *Phys. Rev. Lett.* **74**, 4091 (1995).
 [2] H. C. Nägerl, D. Leibfried, H. Rohde, G. Thalhammer, J. Eschner, F. Schmidt-Kaler, and R. Blatt, *Phys. Rev. A* **60**, 145 (1999).
 [3] R. Scheunemann, F. S. Cataliotti, T. W. Hänsch, and M. Weitz, *Phys. Rev. A* **62**, 051801 (2000).
 [4] R. Dumke, M. Volk, T. Mütter, F. B. J. Buchkremer, G. Birkl, and W. Ertmer, *Phys. Rev. Lett.* **89**, 097903 (2002).
 [5] C. Knoernschild, X. L. Zhang, L. Isenhower, A. T. Gill, F. P. Lu, M. Saffman, and J. Kim, *Appl. Phys. Lett.* **97**, 134101 (2010).
 [6] S. Seidelin, J. Chiaverini, R. Reichle, J. J. Bollinger, D. Leibfried, J. Britton, J. H. Wesenberg, R. B. Blakestad, R. J. Epstein, D. B. Hume *et al.*, *Phys. Rev. Lett.* **96**, 253003 (2006).
 [7] S. C. Doret, J. M. Amini, K. Wright, C. Volin, T. Killian, A. Ozakin, D. Denison, H. Hayden, C.-S. Pai, R. E. Slusher *et al.*, *New J. Phys.* **14**, 073012 (2012).
 [8] S. X. Wang, J. Labaziewicz, Y. Ge, R. Shewmon, and I. L. Chuang, *Appl. Phys. Lett.* **94**, 094103 (2009).
 [9] C. Zhang, S. L. Rolston, and S. Das Sarma, *Phys. Rev. A* **74**, 042316 (2006).
 [10] P. Kunert, D. Georgen, L. Bogunia, M. Baig, M. Baggash, M. Johanning, and C. Wunderlich, *Appl. Phys. B* **114**, 27 (2014).
 [11] P. Staunum and M. Drewsen, *Phys. Rev. A* **66**, 040302 (2002).
 [12] C. Weitenberg, M. Endres, J. F. Sherson, M. Cheneau, P. Schauß, T. Fukuhara, I. Bloch, and S. Kuhr, *Nature (London)* **471**, 319 (2011).
 [13] U. Warring, C. Ospelkaus, Y. Colombe, R. Jördens, D. Leibfried, and D. J. Wineland, *Phys. Rev. Lett.* **110**, 173002 (2013).
 [14] J. H. Lee, E. Montano, I. H. Deutsch, and P. S. Jessen, *Nat. Commun.* **4**, 2027 (2013).
 [15] C. Shen, Z.-X. Gong, and L.-M. Duan, *Phys. Rev. A* **88**, 052325 (2013).
 [16] S. S. Ivanov and N. V. Vitanov, *Opt. Lett.* **36**, 1275 (2011).
 [17] J. T. Merrill and K. R. Brown, *Adv. Chem. Phys.* **154**, 241 (2014).
 [18] K. R. Brown, A. W. Harrow, and I. L. Chuang, *Phys. Rev. A* **70**, 052318 (2004).
 [19] G. H. Low, T. J. Yoder, and I. L. Chuang, *Phys. Rev. A* **89**, 022341 (2014).
 [20] See Supplemental Material at <http://link.aps.org/supplemental/10.1103/PhysRevA.90.040301> for table of pulse angles and phases.
 [21] G. Vittorini, K. Wright, K. R. Brown, A. W. Harter, and S. C. Doret, *Rev. Sci. Instrum.* **84**, 043112 (2013).
 [22] A. Khromova, C. Piltz, B. Scharfenberger, T. F. Gloger, M. Johanning, A. F. Varón, and C. Wunderlich, *Phys. Rev. Lett.* **108**, 220502 (2012).
 [23] C. Kabytayev, T. J. Green, K. Khodjasteh, M. J. Biercuk, L. Viola, and K. R. Brown, *Phys. Rev. A* **90**, 012316 (2014).
 [24] S. Wimperis, *J. Magn. Reson.* **109**, 221 (1994).
 [25] J. M. Gambetta, A. D. Córcoles, S. T. Merkel, B. R. Johnson, J. A. Smolin, J. M. Chow, C. A. Ryan, C. Rigetti, S. Poletto, T. A. Ohki *et al.*, *Phys. Rev. Lett.* **109**, 240504 (2012).